

# Vacuum ultraviolet oscillator strengths of Hg measured by sum-frequency mixing

A. V. Smith and W. J. Alford

Sandia National Laboratories, Albuquerque, New Mexico 87185

(Received 12 November 1985)

We have measured oscillator strengths for the transitions  $6^1S$  to  $(5d^{10}6s np) n^{1,3}P_1$  for  $n=6$  to 13 and to  $(5d^96s^26p) 6p'^1P$  for atomic Hg. Two new techniques for measuring dispersion based on nonlinear-optical sum-frequency mixing are used to achieve 10% accuracy for the stronger transitions. One method uses crossed beams in a Hg heat-pipe cell to map dispersion curves in regions of anomalous dispersion. The second method uses input beams of three separate frequencies and maps regions of normal and anomalous dispersion by tuning one of the input frequencies to the red and blue of the  $6^3P_1$  level. Because the dispersion of the refractive index near a resonance is determined over a large wavelength range, the oscillator strength of that resonance is determined independent of the strengths of other transitions.

## I. INTRODUCTION

Measurement of atomic oscillator strengths or  $f$  values by nonlinear-optical frequency mixing has been demonstrated by a number of authors.<sup>1-4</sup> These measurements are based on the fact that maximum sum-frequency generation is observed when certain restrictions on the refractive indices are met. For example, for collinear plane-wave inputs at frequencies  $\omega_1$ ,  $\omega_2$ , and  $\omega_3$  and an output frequency  $\omega_4 = \omega_1 + \omega_2 + \omega_3$ , the intensity at  $\omega_4$  maximizes when  $\Delta k = k_4 - k_3 - k_2 - k_1 = 0$ ; that is, when the wave vector of the  $\omega_4$  wave,  $k_4$ , is equal to the wave vector of the atomic polarization at frequency  $\omega_4$  driven by the input waves, i.e.,  $k_1 + k_2 + k_3$ . Such index matching can be achieved in a number of ways. For example, if  $\omega_4$  lies near a resonance of the nonlinear medium, index matching will be achieved, at a particular frequency near the resonance, because of the strong dispersion of  $\omega_4$  there. By measuring the frequency of this  $\Delta k = 0$ , or zero-crossing, point, one can, under favorable conditions, deduce the oscillator strength of the transition from the ground state to the near-resonant state. This technique has the advantage that in a pure atomic vapor, the zero-crossing point is nearly independent of density at sufficiently high density. Absolute density measurements are thus unnecessary. This method was used by Wynne *et al.*<sup>3</sup> to measure Ca oscillator strengths and by Mahon *et al.*<sup>4</sup> to measure Hg oscillator strengths.

A second way to achieve index matching is to mix two gases, one normally dispersive and one anomalously dispersive. Puell *et al.*<sup>2</sup> used a mixture of Xe and Rb to determine the refractive index of Rb at a single frequency and deduce from that an  $f$  value. Kramer *et al.*<sup>1</sup> determined the index-matching frequency for various mixtures of Xe and Ar to map the dispersion of Xe near the  $7s[\frac{3}{2}]_1$  resonance and thereby derive an  $f$  value. For these techniques, the refractive index of the companion gas and the density ratios must be known.

In this paper, we introduce two additional techniques of index matching to the measurement of  $f$  values and obtain highly accurate values for the  $6^1S - n^{1,3}P_1$  ( $n = 6-13$ )

series for atomic Hg. The first method, the crossed-beam method, employs crossed input beams of two frequencies ( $a$  in Fig. 1) with changes in crossing angle producing changes in the frequency of the index-matching point. This allows us to map the dispersion curve of Hg in regions of anomalous dispersion near the  $P$  states of Hg. To obtain  $f$  values from these curves, the absolute Hg density must be known. The second method, the three-laser method, uses parallel beams but the index-matching frequency is varied by changing the detuning of  $\omega_1$  from  $6^3P_1$  ( $b$  in Fig. 1). This allows mapping of the dispersion

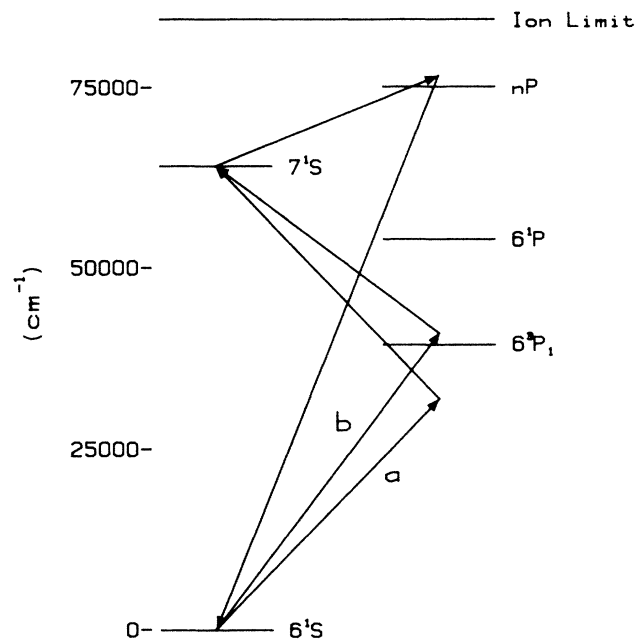


FIG. 1. Partial mercury energy-level diagram showing the two mixing schemes for producing vuv light. Both methods are two-photon resonant with  $7^1S$ . The crossed-beam method ( $a$ ) uses equal photons to reach the  $7^1S$  while for the three-laser method ( $b$ ) we tune one laser near the  $6^3P_1$  level.

curves in regions of normal as well as anomalous dispersion. Another advantage of this method is that the determination of  $f$  values does not require knowledge of the Hg density.

For both methods, a substantial portion of the dispersion curve near a resonance is mapped. This makes possible reliable measurement of the  $f$  value based on the shape of the curve, independent of other transitions. In contrast, when index matching at only a single frequency is determined, it is necessary to know all other  $f$  values which contribute significantly at that frequency.

Our measurements are accurate to about 10% for the stronger Hg transitions. This represents a significant improvement in accuracy for all transitions except  $6^1S-6^1P_1$  and  $-6^3P_1$ . Previous experimentally measured  $f$  values for other transitions from  $6^1S$  appear to be good to only a factor of 2. Reliable theoretical calculations of these  $f$  values could not be found. Considering the importance of Hg to optical and atomic studies, and, more recently, its applications in vacuum ultraviolet (vuv) light generation by nonlinear mixing, the results reported here become increasingly important. Furthermore, the techniques that we report here should also be applicable to a variety of other gases.

The remainder of this paper contains a brief exposition of the theory of index matching in nonlinear mixing in Sec. II, a description of the experimental equipment and methods in Sec. III, a presentation and discussion of results in Sec. IV, and a conclusion in Sec. V.

## II. BACKGROUND

In this section, we present a discussion of the expressions describing three-photon sum-frequency mixing in an atomic vapor. We first consider sum-frequency mixing with parallel, unfocused beams. For this case, the sum-frequency intensity is given by<sup>5</sup>

$$I_4 \sim L^2 N^2 I_1 I_2 I_3 \left| \chi^{(3)}(-\omega_4; \omega_1, \omega_2, \omega_3) \right|^2 \times \left[ \frac{\sin(\Delta k L / 2)}{\Delta k L / 2} \right]^2, \quad (1)$$

where  $\omega_4 = \omega_1 + \omega_2 + \omega_3$ ,  $N$  is the atomic density,  $\Delta k = k(\omega_4) - k_1(\omega_1) - k_2(\omega_2) - k_3(\omega_3)$ ,  $\hat{z}$  is the direction of  $\mathbf{k}_4$ ,  $k(\omega) = n(\omega)\omega/c$ ,  $n(\omega)$  is the index of refraction at frequency  $\omega$ ,  $L$  is the length of atomic vapor,  $\chi^{(3)}$  is the third-order susceptibility, and  $I_n$  is the intensity at frequency  $\omega_n$ . We have assumed that the vapor has a uniform density  $N$  over a length  $L$ . If this is not the case, the product  $NL$  is replaced by  $\int N(z) dz$  and  $\Delta k L$  by  $\int \Delta k(z) dz$ . We have also assumed negligible absorption of  $I_n$  and a weak intensity  $I_4$ . The sinc function in large parentheses is an index-matching factor arising from the sum of electric field contributions over all points from 0 to  $L$ . Restricting ourselves to the case where  $\omega_1 + \omega_2$  is nearly resonant with the intermediate state  $|i\rangle$ ,  $\chi^{(3)}$  is given by the following:

$$\chi^{(3)}(-\omega_4; \omega_1, \omega_2, \omega_3) \sim \sum_{e, e'} \left[ \frac{\langle e' | d | g \rangle}{E_{e'} - \hbar\omega_1 - i\gamma_{e'}} + \frac{\langle e' | d | g \rangle}{E_{e'} - \hbar\omega_2 - i\gamma_{e'}} \right] \frac{\langle i | d | e' \rangle}{E_i - \hbar(\omega_1 + \omega_2) + i\gamma_i} \frac{\langle e | d | i \rangle}{E_e - \hbar\omega_4 - i\gamma_e} \langle g | d | e \rangle, \quad (2)$$

where  $|g\rangle$  is the ground state,  $|e\rangle$  and  $|e'\rangle$  are states one-photon connected to the ground state,  $d$  is the dipole operator, and  $\gamma_n$  is the half-width of  $|n\rangle$ . The index of refraction is given by

$$n(\omega) = 1 + 2\pi N \alpha(\omega), \quad (3)$$

where  $\alpha(\omega)$  is the atomic polarizability at frequency  $\omega$ ,

$$\alpha(\omega) = \frac{e^2}{m} \sum_n \left[ \frac{f_{gn}}{\omega_n^2 - \omega^2} + \int \frac{df}{d\omega_c} \frac{d\omega_c}{\omega_c^2 - \omega^2} \right], \quad (4)$$

$$df/d\omega_c = \frac{mc}{2\pi^2 e^2} \sigma(\omega) \quad (5)$$

(cgs units).  $\sigma(\omega)$  is the continuum photoabsorption cross section. The absorption oscillator strength, or absorption  $f$  value, is given by  $f_{gn}$ ,

$$f_{gn} = \frac{2m\omega_{ng}}{3\hbar e^2 g_g} \sum_{m_g, m_n} |\langle n, m_n | d | g, m_g \rangle|^2, \quad (6)$$

where  $g_g$  is the degeneracy of the ground state and the sum is over magnetic sublevels. The sum in Eq. (4) is over all bound states;  $\hbar\omega_n$  being the energy of  $|n\rangle$ . The integral in Eq. (4) is over the entire continuum.

The above expressions show that the atomic oscillator

strengths enter the expression for sum-frequency mixing, Eq. (1), in both the susceptibility and the index-matching factor. If  $\chi^{(3)}$  is not a strongly varying function of  $\omega_4$ , then the peak intensity will occur at a frequency such that  $\Delta k = 0$ , i.e., where the index-matching factor is a maximum. Both methods for measuring oscillator strengths discussed below take advantage of the sensitivity of the index-matching factor to various oscillator strengths as  $\omega_4$  is varied.

The crossed-beam method uses the same input beam for  $\omega_1$  and  $\omega_2$  [ $\omega_1 = \omega_2 = E(7^1S)/2\hbar$ ] and a second input beam for  $\omega_3$  ( $a$  in Fig. 1). This method requires the beams to be crossed at a small, variable angle  $\theta$  (see Fig. 2). If the two beams are not parallel, then, strictly speak-

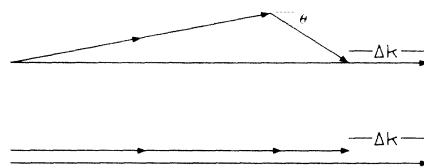


FIG. 2. Addition of wave vectors for sum-frequency mixing. Upper figure is for two crossed beams while the lower figure is for parallel beams.

ing, the index-matching factor in Eq. (1) will be a more complicated function of  $\Delta k$  dependent on beam geometry and overlap. However, for a given trajectory parallel to  $\mathbf{k}_4$ , the propagation direction for the  $\omega_4$  wave, maximum sum-frequency output occurs when the propagation vector of the nonlinear polarization,  $2\mathbf{k}_1 + \mathbf{k}_3$ , is equal to  $\mathbf{k}_4$ , i.e.,  $\Delta k = 0$ . Different trajectories will have different vapor lengths, but each trajectory will yield maximum sum-frequency generation for  $\Delta k = 0$ . Crossing the beams introduces a positive  $\Delta k$ , as indicated in Fig. 2. For small angles, this is given by

$$\Delta k_{\text{crossing}} = k_1 + k_2 + k_3 - |\mathbf{k}_1 + \mathbf{k}_2 + \mathbf{k}_3|, \quad (7)$$

$$\Delta k_{\text{crossing}} = \frac{k_1 k_3}{2k_1 + k_3} \theta^2$$

and is independent of mercury density to a very good approximation. Note that for difference-frequency mixing,  $k_3$  is replaced by  $-k_3$  in Eq. (7). For convenience, we define  $\Delta k^*(\omega_4)$  as  $\Delta k$  for the case of parallel beams and  $\omega_1 = \omega_2 = E(7^1S)/2\hbar$ , and mercury density,  $N_0$ , of  $2.41 \times 10^{16} \text{ cm}^{-3}$ :

$$\Delta k^*(\omega_4) = k(\omega_4) - 2k(E(7^1S)/2\hbar) - k(\omega_3). \quad (8)$$

Thus,  $\Delta k^*(\omega_4)$  is a function of  $\omega_4$  and  $\omega_3$ , but since  $\omega_3$  is weakly dispersed, it is approximately equal to  $k(\omega_4) + \text{const}$ . For a given crossing angle and mercury density, the sum-frequency maximum will occur at the frequency  $\omega^*$  where  $\Delta k = 0$ ,

$$\Delta k = \frac{N}{N_0} \Delta k^*(\omega^*) + \Delta k_{\text{crossing}} = 0$$

or

$$\frac{N}{N_0} \Delta k^*(\omega^*) = -\Delta k_{\text{crossing}} \quad (9)$$

since the atomic medium must cancel the positive  $\Delta k$  due to the beam crossing. Thus, using the crossed-beam technique, one can map out  $\Delta k^*(\omega_4) < 0$  for a particular mercury density by varying the crossing angle and finding the frequency  $\omega^*$  corresponding to maximum sum-frequency generation for each angle. If the mercury density is known, the  $f$  value can be determined from the shape of  $\Delta k^*(\omega_4)$ . The angles necessary for our experiment in mercury are small, less than  $2^\circ$ .

The three-laser method uses parallel, collimated beams with  $\omega_1 \neq \omega_2 \neq \omega_3$ . For example, using a fixed  $\omega_1$  and  $\omega_2$  such that  $\omega_1 + \omega_2 = E(7^1S)/\hbar$  with  $\omega_1$  near  $E(6^3P_1)/\hbar$ , we can scan  $\omega_3$  so that  $\omega_4$  is near  $E(9^1P)/\hbar$ . Maximum sum-frequency generation will occur at a frequency  $\omega^*$  for which  $\Delta k = 0$ . Since  $k_1 + k_2 = k_4 - k_3$  when  $\Delta k = 0$ , we can express Eq. (8) in the form

$$\Delta k^*(\omega^*) = k(\omega_1) + k(\omega_2) - 2k(E(7^1S)/2\hbar), \quad (10)$$

where the right-hand side is calculated for a mercury density of  $N_0$ . In general, the right-hand side of this equation can be positive or negative and is a strong function of the detuning of  $\omega_1$  from  $6^3P_1$ . The tuning of  $\omega_1$  away from  $\omega_1 = E(7^1S)/2\hbar$  provides the change in  $\Delta k^*(\omega_4)$  just as a nonzero angle produced a change in the crossed-beam

method. The experimental procedure is to find  $\omega^*$  for a variety of settings of  $\omega_1$ . Since both sides of Eq. (10) are proportional to  $N_0$ , it follows that  $\omega^*$  depends on  $\omega_1$ , but is independent of mercury density. The function  $\Delta k^*(\omega_4)$  can be mapped over large regions (hundreds or thousands of wave numbers) of  $\omega_4$ . Knowing  $\Delta k^*(\omega_4)$  near a particular  $nP$  state, one can then fit the data by varying the oscillator strength for the  $6^1S - nP$  transition. These  $f$  values are then used in a second iteration to evaluate the right-hand side of Eq. (4) and to obtain an improved set of  $f$  values.

We have assumed that the third-order susceptibility is not a strongly varying function of  $\omega_4$  in the region of  $\Delta k = 0$ . This may or may not be a good approximation. When  $\omega_4$  is close to a resonance, we see from Eq. (2) that

$$|\chi^{(3)}|^2 \sim \frac{1}{\Delta^2 + \gamma^2}, \quad (11)$$

where  $\Delta$  is the detuning from resonance. Often  $\Delta \gg \gamma$ , but still small enough to use Eq. (11). In this case,

$$I_4 \sim \frac{1}{\Delta^2} \left[ \frac{\sin(\Delta k L / 2)}{\Delta k L / 2} \right]^2. \quad (12)$$

Thus, the observed sum-frequency signal will be a maximum at a frequency,  $\omega_4$ , that has been shifted toward the resonance. It is often the case that the sum-frequency-mixing peak is narrow enough that the shape of  $\chi^{(3)}$  is not important. In general, however, one must consider the shape of  $\chi^{(3)}$  when finding the frequency at which  $\Delta k = 0$ . Ideally, one would like to know the shape of  $\chi^{(3)}$  in order to determine the  $\Delta k = 0$  frequency. Near strong transitions we have found Eq. (12) to be valid but near weak transitions Eq. (12) is not a good approximation and the shape of  $\chi^{(3)}$  is not known well.

An advantage of the present methods is that the shape of the  $\Delta k^*(\omega_4)$  curve rather than a single point on this curve is used to determine oscillator strengths. This is an important point since the frequency at which  $\Delta k^*(\omega_4) = 0$  can be sensitive to other bound- and continuum-state transitions. Thus, one must be sure these other transitions are properly accounted for, or negligible, when using a single point to determine oscillator strengths.

### III. EXPERIMENTAL SETUP

A diagram of the experimental setup used for the crossed-beam experiment is shown in Fig. 3. The three-laser experiment uses a third dye laser not shown in Fig. 3. The outputs of two Nd:YAG-pumped dye lasers (where YAG is yttrium aluminum garnet) are sent unfocused into a mercury heat-pipe cell. Sum-frequency output from the mercury cell is separated from the laser frequencies using a LiF prism and is detected with a photomultiplier.

The mercury cell is a stainless-steel cross heated in the middle and water cooled at the windows. A side view of one arm of the cell is shown in Fig. 4(a). Each arm has a 23-cm conical section (0.8 mm wall thickness) which provides gravity recirculation of the condensed mercury. The cell contains about  $15 \text{ cm}^3$  of liquid mercury and has been

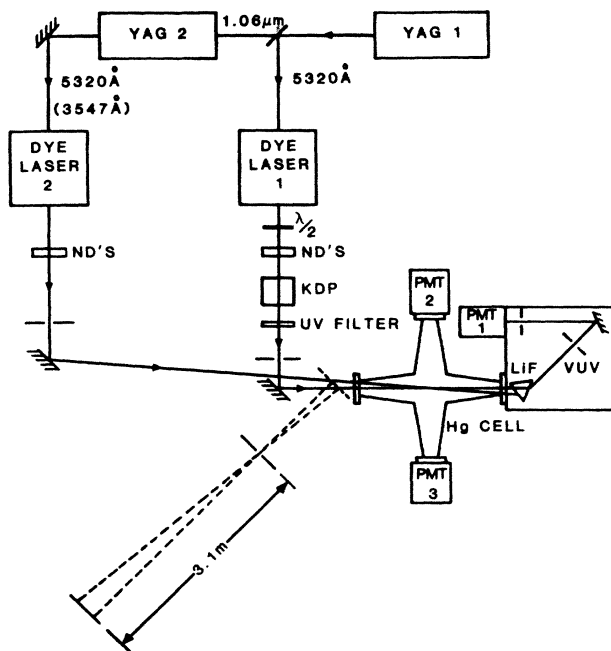


FIG. 3. Experimental setup for the crossed-beam measurement.

used for about three months with no coating of the windows or other problems. Each arm is heated for the first 8 cm from the middle [0–8 cm in Fig. 4(a)] and has alumina-silica insulation extending out 22 cm. A metal-vapor heat-pipe cell is characterized by a pure metal vapor in the central portion with a pressure determined by the pressure of an inert buffer gas in the end regions.<sup>6</sup> We

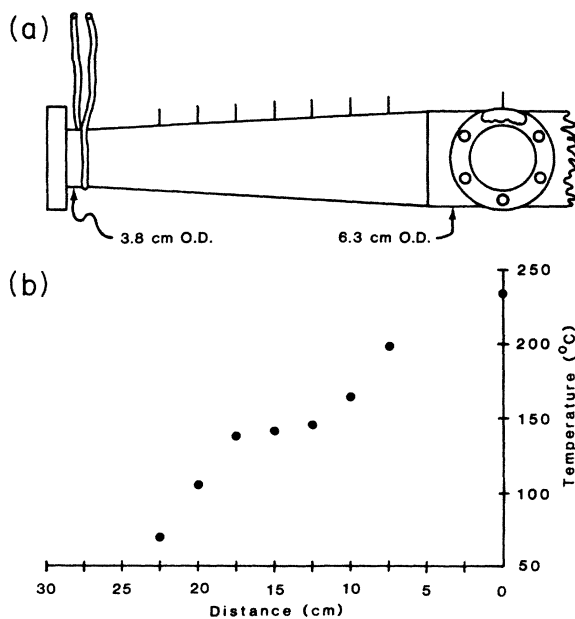


FIG. 4. (a) Side view of one arm of the mercury cell. (b) Temperature distribution measured with thermocouples on the outside of the cell for a buffer-gas pressure of 3.5 torr. O.D. is the outer diameter.

have shown by Rayleigh scattering<sup>7</sup> measurements that within the 15% measurement accuracy the Hg pressure follows the He buffer-gas pressure over a range of 1–4 torr. Figure 4(b) shows a temperature profile of one arm of the cell obtained with thermocouples attached (spot welded and covered with heat-resistant cement) to the top of the cell. This profile is for a He buffer-gas pressure of 3.5 torr. The temperature distribution does not show the flat distribution common to other heat-pipe designs.<sup>6</sup> However, the observed shoulder in the temperature distribution at about 150°C is due to convective heating by mercury vapor, or “heat piping.” At 155°C, the Hg vapor pressure is 3.5 torr. The excess temperature at the cell center reflects the fact that we do not efficiently heat the liquid mercury. This may be due to the low thermal conductivity of mercury (relative to the alkali metals) and possibly the fact that mercury does not wet stainless steel to make good thermal contact with the walls.

The Rayleigh scattering measurements were made at the center of the cell. The cross section for Rayleigh scattering by a <sup>1</sup>S ground state is given by

$$\frac{d\sigma}{d\Omega} = \alpha^2(\omega) k^4(\omega) (\hat{\epsilon} \cdot \hat{\epsilon}_s)^2,$$

where  $\hat{\epsilon}$  and  $\hat{\epsilon}_s$  are the incident and scattered polarizations. We calibrated the detection system by first Rayleigh scattering from a known density of krypton for which  $\alpha(\omega)$  is known.<sup>8</sup> We then measured the intensity of the Rayleigh scattering from Hg at the same frequency. Since the ratio  $\alpha_{\text{Hg}}/\alpha_{\text{Kr}}$  is known, the mercury density can be determined. We calculated  $\alpha(\omega)$  for mercury using measured  $6^1S-nP$  oscillator strengths and adjusted Berkowitz photoabsorption data.<sup>9</sup> (See discussion in Sec. IV.) The wavelengths used for the Rayleigh scattering measurements were slightly to the blue side of the  $6^1S-6^3P_1$  intercombination line at 253.7 nm. Since we used a broad bandpass filter to observe the Rayleigh scattering, we

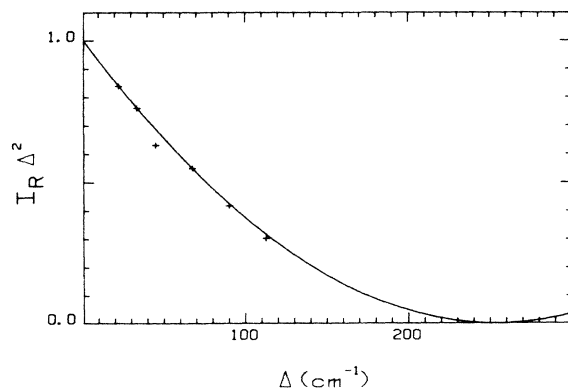


FIG. 5. Rayleigh scattering signal ( $I_R$ ) multiplied by the square of the detuning as a function of detuning (to the blue side) from  $6^3P_1$ . The data (+) are normalized to the calculated curve at  $\Delta = 33.8 \text{ cm}^{-1}$ .

TABLE I. Various dyes and mixing schemes used input beams for mixing in Hg. KDP is potassium dihydrogen phosphate. KD\*P is deuterated KDP.

Wavelength (nm)	Dye, mixing
170 ( $7^1S-7^3P_1$ )	DCM, 1.06 $\mu\text{m}$ in $\text{LiIO}_3$ ( $21^\circ$ )
1360 ( $7^1S-7^1P_1$ )	R640, 1.06 $\mu\text{m}$ in $\text{LiIO}_3$ ( $21^\circ$ )
798 ( $7^1S-8^3P_1$ )	LDS 820
773 ( $7^1S-8^1P_1$ )	LDS 751
672-624 ( $7^1S-6p'^1P, 9^{3,1}P_1$ )	DCM
589-580 ( $7^1S-10^{3,1}P_1$ )	R610
559-555 ( $7^1S-11^{3,1}P_1$ )	F548 + NaOH
542-529 ( $7^1S-12^{3,1}P_1, 13^{3,1}P_1$ )	C500
408 ( $6^3P_1-7^1S$ )	DCM, 1.06 $\mu\text{m}$ in KD*P ( $58^\circ$ )
313 ( $6^1S-7^1S$ , two photons)	DCM, KDP ( $54^\circ$ )
254 ( $6^1S-6^3P_1$ )	DCM, doubled in KDP ( $54^\circ$ ) and Mixed with 1.06 $\mu\text{m}$ in KDP ( $62^\circ$ )

could not use frequencies to the red side of  $6^3P_1$  without interference from mercury dimers.<sup>10</sup> The dependence of the Rayleigh signal on detuning to the blue side of  $6^3P_1$  is shown in Fig. 5 along with the calculated curve, thus confirming that we are measuring Rayleigh scattering.

We next consider the density uniformity and vapor length in the heat-pipe cell. Using parallel beams in the three-laser experiment and calculated values of  $\Delta k^*(\omega_4)$ , we deduce from the positions of the nulls of the sinc function in the observed sum-frequency-mixing signal a total vapor length of 36 cm, assuming the density is uniform and given by that at the center of the cell. This assumption is consistent with visual observation of a broad (3-5 cm) condensation zone at 18-20 cm from the cell center and with the measured temperature distribution shown in Fig. 4(b). We believe that the Hg pressure is constant inside 18 cm but because the temperature diminishes from cell center to 18 cm, the Hg density may rise slightly away from the center. The maximum increase would be less than 20%. This will be included in our estimate of the total uncertainty of our measured  $f$  values. Experimentally, we find that the two methods used for determining oscillator strengths, one of which is independent of density, agree very well if we assume the density is that derived from the measured He pressure and the temperature at the cell center.

The Nd:YAG lasers shown in Fig. 3 are Quanta Ray models No. DCR1 and No. DCR2. YAG 2 is used as an amplifier of the 1.06- $\mu\text{m}$  light left over after frequency doubling of YAG 1. Each frequency-doubled Nd:YAG laser pumps a Quanta Ray PDL dye laser having a bandwidth of  $\sim 0.5 \text{ cm}^{-1}$  (full width at half maximum). Table I lists the various dyes and mixing schemes used to produce the light over the range 250-1700 nm used as input beams for mixing in Hg. The output of each dye laser is attenuated with neutral-density filters (ND's in Fig. 3) so that the sum-frequency signal is not strongly saturated. An aperture restricts the diameter of each beam to 2 mm. Typical power densities of the vertically polarized light entering the Hg cell are 0.2 MW/cm<sup>2</sup> and 2 MW/cm<sup>2</sup> from dye lasers 1 and 2. We estimate a population in the  $7^1S$  state due to two-photon absorption to be less than

$10^{-4}$  of the ground-state population at the end of the laser pulse. The wavelength calibration of the lasers is generally obtained by using laser-induced fluorescence on available resonances. For example,  $7^1S-n^1P$  resonances are found by maximizing the  $7^3S-6^3P_1$  fluorescence which occurs due to transfer of  $n^1P$  population to the triplet manifold by collisional and radiative processes. The photomultiplier tubes (PMT) No. 2 and No. 3 (see Fig. 3) are used for observing such fluorescence. The overall uncertainty in the frequencies of sum-frequency generation maxima due to laser-wavelength accuracy is  $\lesssim 2 \text{ cm}^{-1}$ , mainly due to the frequency drift (in time) of the dye lasers.

The vuv sum-frequency light is separated from the input light using a  $60^\circ$  LiF prism. A Hamamatsu model No. R1259 photomultiplier (PMT 1 in Fig. 3) is used to detect the vuv light and operates at a rather low voltage of typically 450 V. For strong vuv signals, the output of the photomultiplier is not linear in the vuv signal. However, this does not present any problems in finding the position of maximum vuv generation. The output of the photomultiplier is sent to a Princeton Applied Research model No. 165 gated integrator which is interfaced to a computer. The computer scans dye laser 2 while recording the vuv signal.

The angle between the two lasers, as indicated in Fig. 3, is measured by noting the separation between beams at a distance of 3.1 m from the crossing region. It is important to know the crossing angle accurately, since an error in the angle corresponds to an error in  $\Delta k^*$ . Typically, errors in the angle as small as  $0.1^\circ$  can lead to a bad measurement. We estimate the uncertainty in our angle measurements to be  $0.02^\circ$ . The point of maximum beam overlap is at the center of the Hg cell.

#### IV. RESULTS AND DISCUSSION

Figure 6 shows typical data for the crossed-beam and three-laser techniques. The scans here are just to the blue side of the  $10^1P$  level. The frequencies of the signal maxima are plotted in Fig. 7 versus the  $\Delta k^*$  calculated from the crossing angles for the crossed-beam method or from

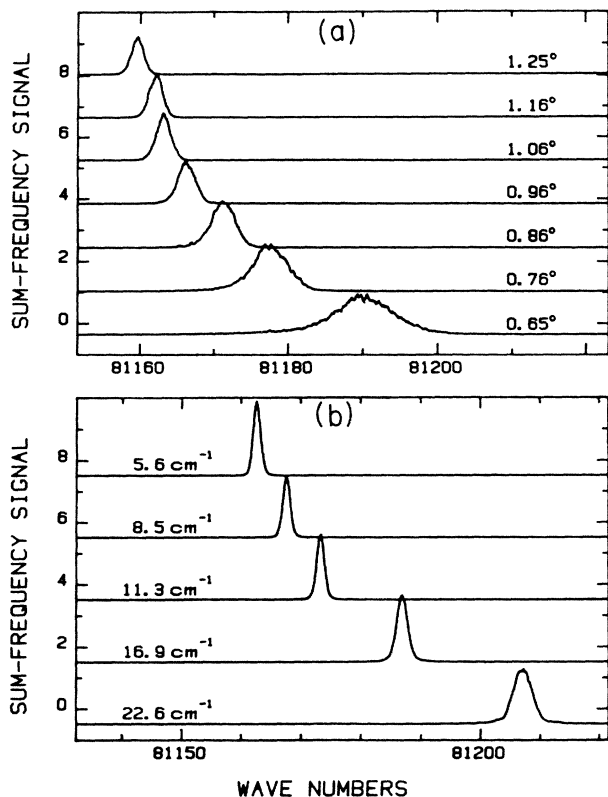


FIG. 6. (a) Observed sum-frequency signal for various crossing angles in the crossed-beam measurements.  $\omega_1 + \omega_2 = E(7^1S)/2\hbar$ ,  $\omega_3$  variable. (b) Observed sum-frequency signal for various detunings of  $\omega_1$  to the blue of  $6^3P_1$  in the three-laser measurements.  $\omega_1 + \omega_2 = E(7^1S)/h$ ,  $\omega_3$  variable.

the detuning from  $6^3P_1$  for the three-laser method. The solid curve is our best fit to the data and yields the tabulated  $f$  value of  $10^1P$ . Only the  $8^{1,3}P_1$  and  $10^1P$   $f$  values were measured using the three-laser method. The agreement between the two methods for the  $8^1P$  and  $10^1P$   $f$  values is better than 5%, while for the  $8^3P_1$  it is about

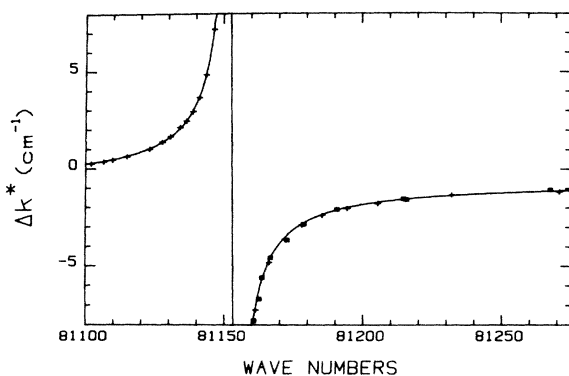


FIG. 7.  $\Delta k^*(\omega_4)$  (approximately the dispersion at frequency  $\omega_4$ ) as a function of energy near  $10^1P$ . Data points are the observed peak positions from scans like those shown in Fig. 6. Squares (crosses) are from the crossed-beam (three-laser) measurements. Solid curve corresponds to the  $f$  value giving the best fit to the data.

15%. All other values reported here were obtained using the crossed-beam method. All data and calculated curves shown are normalized to a Hg density of  $2.41 \times 10^{16} \text{ cm}^{-3}$  (1 torr at 400 K). All data was taken at pressures of 3.3–3.5 torr and a temperature of about 235°C. These data are then fit using Eqs. (3) and (4) to calculate  $\Delta k^*$  for various trial  $f$  values and visually determining a best value. The polarizability for all four frequencies is calculated using Eq. (4) with the measured  $f$  values for  $6^1S-n^{1,3}P_1$  ( $n=6-13$ ) and the proper continuum contribution (see discussion below). Thus, we use an iterative process for obtaining a complete set of  $f$  values. Because a dispersion shape is measured, the  $f$  value determined this way is not very sensitive to other  $f$  values. They will simply contribute to a vertical offset for the computed curve and it is largely this vertical offset which is fit by iteration. We have used the data of Baig<sup>11</sup> for mercury energy levels. Our results are listed in Table II along with previous measurements. The  $7^3P_1$  dispersion was too weak to map using our present methods. Only an upper limit based on our laser-bandwidth-limited resolution of  $10^{-5}$  was possible.

An idea of the uncertainty associated with determining an  $f$  value from our data may be gained by studying Fig. 8. Here, data near the  $12^3P_1$  and  $12^1P$  lines are used to determine  $6^1S-12^3P_1$  and  $6^1S-12^1P$   $f$  values. The solid curve is our best fit ( $f_1=0.0023$ ,  $f_3=0.0008$ ) while the dashed line is at the estimated outer bound of our fitting error ( $f_1=0.0020$ ,  $f_3=0.0010$ ). These fitting uncertainties combined with other sources of uncertainty to be discussed later are reflected in the total uncertainties listed in Table II.

The fitting uncertainties are largely due to the uncertainty in laser calibration of approximately  $1-2 \text{ cm}^{-1}$ . This leads to possible errors in measured  $f$  values ranging from 30% for the weakest transitions measured to less than 10% for the stronger ones. For crossed beams, additional contributions to the total uncertainty arise from uncertainty in the Hg density and the effects of nonuniform Hg density, from uncertainty in the crossing angles, from shifts in measured peak positions due to the frequency dependence of  $\chi^{(3)}$ , and from contributions to the refractive indices due to excited-state population and  $\text{Hg}_2$  molecules.

We believe the Hg density near the center of the oven is known to be about 5% based on the excellent agreement of our measured  $f$  value for the  $6^1S-6^3P_1$  transition with lifetime measurements for  $6^3P_1$  and the consistency of our  $6^1S-8^{1,3}P_1, 10^1P$   $f$  values measured by the crossed-beam and three-laser techniques. Because of the temperature profile of our cell, we expect that the Hg density 15 cm from cell center will be greater than at the cell center by as much as 20%. This could distort our data for angles less than one degree for which the beam overlap exceeds 10 cm. This corresponds to a  $\Delta k^* > -4 \text{ cm}^{-1}$ . However, it appears that even for considerably smaller angles than this, the nonuniformity actually is not very important. Since the beam overlap is greatest at the cell center and tapers off on either side, the effective overlap is considerably less than the maximum calculated overlap. The effective mixing length can be estimated from the

TABLE II. Measured absorption oscillator strengths from  $6^1S$  ground state.

Upper level	$^1P_1$			$^3P_1$		$\frac{f(^3P_1)}{f(^1P_1)}$
	Present work	Mahon and Tomkins (Ref. 4)	Skerbele <i>et al.</i> (Ref. 20)	Present work	Others	
$6P$	1.15		1.11	0.024(10%)	0.024 <sup>b</sup>	0.021
$7P$	0.020(10%)		0.049	$< 10^{-5}$		$< 0.0005$
$8P$	0.0100(12%)		0.021	0.0014(17%)		0.11
$6p^1P$	0.15(10%)		0.24			
$9P$	0.070(10%)	0.0415	0.115	0.0055(10%)		0.079
$10P$	0.0155(10%)	0.0142	0.029	0.0018(20%)		0.12
$11P$	0.0050(15%)	0.0051	0.012	0.0011(20%)		0.22
$12P$	0.0023(15%)			0.0008(30%)		0.35
$13P$	0.0011(15%)			0.0005(35%)		0.45

<sup>a</sup>Weighted average from literature, see Ref. 18.

<sup>b</sup>Weighted average from literature, see Ref. 19.

width of the observed peaks in Fig. 6(a) since the width is inversely proportional to the interaction length. This yields an effective length of only 7 cm for the scan at  $0.65^\circ$  crossing angle corresponding to a  $\Delta k^* = -2 \text{ cm}^{-1}$ . Given the good agreement of the two sets of data in Fig. 7, we conclude that the nonuniformity should contribute less than 5% for  $\Delta k^* < -1 \text{ cm}^{-1}$  and about 5% for  $-1 < \Delta k^* < 0 \text{ cm}^{-1}$ .

The effect of  $\chi^{(3)}$  on the peak positions is considered next. Near a singlet  $P$  state,  $\chi^{(3)}$  is dominated by that state and diminishes inversely as the detuning from resonance, Eq. (12). Thus, to normalize our signals, we must multiply by  $\Delta^2$ . This was done for our  $7P$ ,  $9P$ , and  $12P$  crossed-beam data with the result that each peak was moved about 0.5–1.0 wave numbers towards the blue region for the  $7P$ . For  $9P$ , the shifts are smaller while for  $12P$  they are larger. This effect is largest when the peak width to detuning ratio is greatest, i.e., for small  $f$  values, so it will introduce more uncertainty for weaker transitions. Because all peaks are shifted to some extent, part of the shift is taken up by a small frequency shift in our visual fits. The estimated uncertainties range from negli-

gible for  $6p^1P$  and  $9^1P$  to about 10% for  $13^1P$ . The behavior of  $\chi^{(3)}$  near the triplets is generally more complex than near the singlets since interference creates nulls in  $\chi^{(3)}$  near the triplets on both sides so no simple correction is possible at present. Possible errors range from 20% for  $13^3P_1$  to less than 5% for  $9^3P_1$ .

The angle-crossing error of  $0.02^\circ$  contributes much less to the  $f$  value uncertainty than other sources of error. So does  $7^1S$  excited-state population and the presence of Hg molecules, both of which are present at levels  $10^{-4}$  or less relative to the ground-state density.<sup>12</sup>

For the three-laser measurements, error analysis is much simpler. The density and density profile are not important except in producing a sufficiently narrow index-matching peak. Because the peaks are much narrower than in the crossed-beam method, the effects of the frequency dependence of  $\chi^{(3)}$  are also much smaller so the uncertainty using this technique is due mainly to laser linewidth and calibration errors.

In fitting our data, the  $f$  value is determined from the shape of the dispersion curves. The vertical offset is determined by all the remaining oscillator strength, bound and continuum. Since nearly all the bound-state contribution is accounted for in our measurements, the continuum contribution can be determined from our data. When added to the polarizability due to bound states, the continuum contribution shown in Fig. 9 gives good agreement with our data, with the dc polarizability of  $5.1 \text{ \AA}^3$ ,<sup>13</sup> and with the long-wavelength dispersion data of Wolfsohn.<sup>14</sup> This curve was calculated using Eq. (5) and the data of Brehm,<sup>15</sup> Berkowitz and Lifshitz,<sup>16</sup> and Cairns.<sup>17</sup> (See also Ref. 9.) Some adjustment of their photoionization cross sections was necessary to achieve this agreement. The data of Refs. 15 and 16 were used below  $137000 \text{ cm}^{-1}$  and were multiplied by a factor of 1.2 while the data of Ref. 16 were used above this energy and multiplied by 0.625. These corrections appear to be within the limits of error for these cross sections. The uncertainties of our multipliers is about 20%. As an example of the importance of this continuum contribution; the computed curve in Fig. 7 would be lowered by  $0.2 \text{ cm}^{-1}$  without the continuum contribution, in clear disagreement with the data.

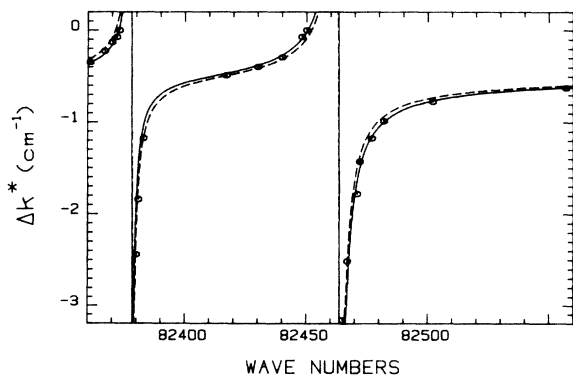


FIG. 8.  $\Delta k^*(\omega_4)$  vs  $\omega_4$  near the  $12^3P_1$  and  $12^1P$  transitions. Data are from the crossed-beam method and the solid curve is our best fit to this data [ $f(^1P)=0.0023$ ,  $f(^3P_1)=0.0008$ ]. Dashed curve shows our estimated uncertainty [ $f(^1P)=0.0020$ ,  $f(^3P_1)=0.0010$ ].

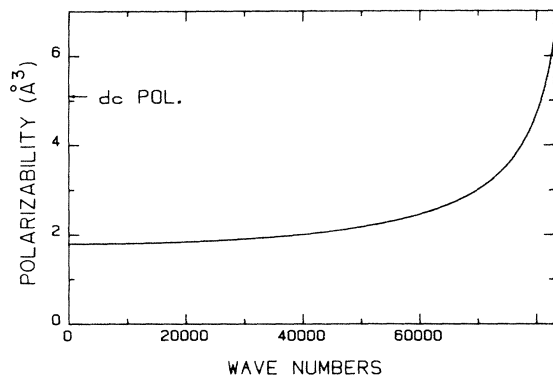


FIG. 9. The polarizability of mercury due to the continuum as a function of energy. See text for a description of the photoabsorption data used to model the continuum. Note that the dc polarizability, which includes bound-state as well as continuum-state contributions, is  $5.1 \text{ \AA}^3$  (Ref. 13).

Earlier experimentally determined  $f$  values for the  $6^1S-n^1,3P_1$  transitions are available for some of the transitions. The  $6^1P$  and  $6^3P_1$   $f$  values are known from a large number of predominantly lifetime measurements<sup>18,19</sup> and a weighted average gives the values listed in Table II. The other values in Table II come from Refs. 4 and 20. The values of Skerbele *et al.*<sup>20</sup> are derived from low-energy electron excitation cross sections. Their results are consistently too high by approximately a factor of 2. The values of Mahon and Tomkins<sup>4</sup> were obtained by sum-frequency mixing with parallel beams to find the  $\Delta k=0$  points. Their  $\Delta k=0$  points are slightly the red of ours which might indicate a slight crossing of the input beams. This does not account for the difference in measured  $f$  values, however. The disagreement between present results and theirs for  $9^1P$  is due mainly to the neglect of contributions from  $6p^1P$  and the continuum in their analysis. Because they measure only a single point on the

dispersion curve, their derived  $f$  values are sensitive to these contributions. For the  $10^1P$  and  $11^1P$ , the continuum and  $6p^1P$  contributions very nearly cancel leading to agreement with our measurements.

From Table II, it is apparent that transitions from  $6^1S$  to the triplets gain in oscillator strength relative to the singlets as  $n$  increases. This trend was also observed by Baig<sup>11</sup> and has been attributed to perturbations by low-lying autoionizing states,<sup>21</sup> particularly the strong autoionizing state at  $88\,760 \text{ cm}^{-1}$  belonging to the  $5d^96s^2$ ,  $J=\frac{3}{2}$  core. The  $6p^1P$  state at  $78\,813 \text{ cm}^{-1}$  belongs to the  $5d^96s^2$ ,  $J=\frac{5}{2}$  core configuration and also perturbs the  $5d^{10}6s np$  series, especially the  $8P$  and  $9P$  states.

## V. CONCLUSIONS

We have demonstrated the utility of two new techniques for the measurement of  $f$  values. Both give dispersion curves rather than a single point on the curve so the measured  $f$  value is relatively independent of the distribution of the remaining oscillator strength. The crossed-beam method is simpler in that it requires fewer lasers but it requires knowledge of atomic density. It also produces broader index-matching peaks due to the shortened overlap region, and it can generate data only in regions of  $\Delta k^* < 0$  for sum-frequency generation or  $\Delta k^* > 0$  for difference-frequency mixing. The three-laser method requires an additional laser but gives better results independent of vapor density or uniformity. The uncertainty in our measurements using this latter technique was mainly determined by the laser linewidth and calibration. Using improved laser sources, we would expect that uncertainties could be reduced to  $\sim 1\%$ .

## ACKNOWLEDGMENT

This work was performed at Sandia National Laboratories and supported by the U.S. Department of Energy under Contract No. DE-AC04-76DP00789 for the Office of Basic Energy Sciences.

<sup>1</sup>S. D. Kramer, C. H. Chen, and M. G. Payne, in *Proceedings of the Second Topical Meeting on Laser Techniques in the Extreme Ultraviolet*, edited by S. E. Harris and T. B. Lucatorto (AIP, New York, 1984).

<sup>2</sup>H. Puell and C. R. Vidal, *Opt. Commun.* **19**, 279 (1976).

<sup>3</sup>J. J. Wynne and R. Beigang, *Phys. Rev. A* **23**, 2736 (1981).

<sup>4</sup>R. Mahon and F. S. Tomkins, *IEEE J. Quantum Electron.* **QE-18**, 913 (1982).

<sup>5</sup>J. F. Reintjes, *Nonlinear Optical Parametric Processes in Liquids and Gases* (Academic, New York, 1984).

<sup>6</sup>C. R. Vidal and J. Cooper, *J. Appl. Phys.* **40**, 3370 (1969).

<sup>7</sup>W. J. Alford, N. Andersen, K. Burnett, and J. Copper, *Phys. Rev. A* **30**, 2366 (1984).

<sup>8</sup>P. J. Leonard, *At. Data Nucl. Data Tables* **14**, 21 (1974).

<sup>9</sup>J. Berkowitz, *Photoabsorption, Photoionization and Photoelectron Spectroscopy* (Academic, New York, 1979).

<sup>10</sup>R. E. Drullinger, M. M. Hessel, and E. W. Smith, *J. Chem. Phys.* **66**, 5656 (1977).

<sup>11</sup>M. A. Baig, *J. Phys. B* **16**, 1511 (1983).

<sup>12</sup>K. Hilpert, *J. Chem. Phys.* **77**, 1425 (1982).

<sup>13</sup>R. R. Teachout and R. T. Pack, *At. Data* **3**, 195 (1971).

<sup>14</sup>G. Wolfsohn, *Z. Phys.* **83**, 234 (1933).

<sup>15</sup>B. Brehm, *Z. Naturforsch. A* **21**, 196 (1966).

<sup>16</sup>J. Berkowitz and C. Lifshitz, *J. Phys. B* **1**, 438 (1968).

<sup>17</sup>R. B. Cairns, H. Harrison, and R. I. Schoen, *J. Chem. Phys.* **53**, 96 (1970).

<sup>18</sup>R. Abjean and A. Johannin-Gilles, *J. Quant. Spectrosc. Radiat. Transfer* **16**, 369 (1976); D. Gebhard and W. Behmenburg, *Z. Naturforsch.* **30a**, 445 (1974); P. D. Lecler, *J. Phys. (Paris)* **29**, 611 (1968); A. Lurio, *Phys. Rev.* **140**, A1505 (1965); A. Skerbele and E. N. Lassette, *J. Chem.* **52**, 2708 (1970); T. Anderson and G. Sorensen, *J. Quant. Spectrosc. Radiat. Transfer* **13**, 369 (1973); G. Wolfsohn, *Z. Phys.* **83**, 234 (1933); C. Bousquet and N. Bras, *J. Phys. (Paris)* **41**, 19 (1980).

<sup>19</sup>K. A. Mohamed, *J. Quant. Spectrosc. Radiat. Transfer* **30**, 225 (1983); J. A. Halstead and R. R. Reeves, *ibid.* **28**, 289 (1982); G. C. King and A. Adams, *J. Phys. B* **7**, 1712 (1974); J. N. Dodd, W. J. Sandle, and O. M. Williams, *ibid.* **2**, 256 (1970); J. S. Deech and W. E. Baylis, *Can. J. Phys.* **49**, 90

(1971); G. H. Nussbaum and F. M. Pipkin, *Phys. Rev. Lett.* **19**, 1089 (1967); J. P. Barratt, *J. Phys. Radium* **20**, 541 (1959); **20**, 633 (1959); **20**, 657 (1959).  
<sup>20</sup>A. Skerbele, K. J. Ross, and E. N. Lassettre, *J. Chem. Phys.*

**50**, 4486 (1969); A. Skerbele and E. N. Lassettre, *ibid.* **52**, 2708 (1970); **56**, 8405 (1972).  
<sup>21</sup>G. Schönhense, F. Schäfers, Ch. Heckenkamp, U. Heinzmann, and M. A. Baig, *J. Phys. B* **17**, L771 (1984).